RESEARCH

The cranium and dentition of *Khirtharia* (Artiodactyla, Raoellidae): new data on a stem taxon to Cetacea

Mohd Waqas[1,2] · Thierry Smith[3] · Rajendra Singh Rana[2] · Maeva J. Orliac[1]

Abstract

Raoellid mammals are small artiodactyls from the Eocene of Asia, hypothesized to be closely related to stem Cetacea. Knowledge of the cranial and dental morphology of Raoellidae comes mostly from one species, *Indohyus indirae*. Here we describe new material of another raoellid genus, *Khirtharia*, based on material retrieved from the Kalakot area, Jammu and Kashmir. This new material, comprising an almost complete, lightly deformed cranium and a partial snout with associated partial mandible, greatly adds to our knowledge of raoellid morphology. It highlights the similarity of cranial characters with *Indohyus*, such as a long snout with raptorial incisors, a thick and narrow supraorbital region, a strong postorbital constriction, a triangular shaped braincase, and a thickened medial wall to the auditory bulla (involucrum). The new specimen is similar to *Indohyus* cranially but differs dentally in being more bunodont. The presence of these traits in two different raoellid genera suggests they may be present more broadly across Raoellidae. These characters are also observed in early cetaceans, highlighting the need to investigate their phylogenetic impact. Some cranial features support aquatic habits of members of this family.

Keywords Cetacea · India · Middle Eocene · Subathu Formation

Introduction

Raoellidae are small artiodactyls from the Eocene of Asia, mostly recovered from the Indian subcontinent (see Orliac and Ducrocq 2012 for a review). Their peculiar dental and cranial features have placed them as sister taxa to stem Cetacea in a number of cladistic analyses (Thewissen et al. 2001, 2007; Geisler and Uhen 2003, 2005; Orliac and Ducrocq 2012; Gatesy et al. 2013; McGowen et al. 2014). Noteworthy is the presence, in the genus *Indohyus*, of an involucrum on the auditory bulla (Thewissen et al. 2007), a derived feature shared with cetaceans and associated with underwater hearing. As raoellids are hypothesized to be freshwater inhabitants (Thewissen et al. 2007; Cooper et al. 2012), the

✉ Maeva J. Orliac
maeva.orliac@umontpellier.fr

1 Institut des Sciences de l'Evolution de Montpellier,
Université de Montpellier, Montpellier, France

2 Department of Geology, HNB Garhwal University,
Srinagar Garhwal 246174, Uttarakhand, India

3 Directorate Earth and History of Life, Royal Belgian Institute
of Natural Sciences, 29 Rue Vautier, 1000 Brussels, Belgium

presence of the involucrum in raoellids documents important steps in the transition from land to sea in Artiodactyla.

Beyond the auditory region, several cranial features of *Indohyus* are shared with cetaceans, such as the peculiar shape of the brain and associated sinuses (Orliac and Thewissen 2021), and the constricted, thick, supraorbital region (Patel et al. 2024). Yet, to date, knowledge of the cranial morphology of Raoellidae has been based only on *Indohyus indirae*. Documenting the cranial morphology of other raoellid species is of great interest to understand whether the cranial anatomy of this clade is as diverse as the dental morphology, which shows different degrees of bunodonty and lophodonty (Theodor et al. 2007; Thewissen et al. 2011; Orliac and Ducrocq 2012). Raoellids were defined as "extremely bunodont forms showing various degrees of lophodonty" (Theodor et al. 2007: p. 56). The family today encompasses five genera and nine species: *Kunmunella* Sahni and Khare, 1971 (two species), *Indohyus* Ranga Rao, 1971 (one species), *Metkatius* Kumar and Sahni, 1985 (one species), *Khirtharia* Pilgrim, 1940 (four species), and *Rajouria* Rana et al., 2021 (one species). A lophodonty gradient is observed from the 'hyperbunodont' molar morphology observed in *Khirtharia* species to sublophodont molars in

Indohyus and *Kunmunella*. Raoellidae are mainly documented by dental remains, *Indohyus indirae* and *Khirtharia dayi* being by far the most abundant taxa in the literature (Kumar and Sahni 1985; Thewissen et al. 1987, 2001, 2020).

We document here the cranial morphology of *Khirtharia inflata* Ranga Rao, 1972, based on exceptionally well-preserved material collected from the East Aiji-2 locality, Rajouri District, Jammu Kashmir, India (Waqas and Rana 2020). The fossiliferous bed is found within the middle Eocene shale of the Upper Subathu Formation (Rana et al. 2021). This new material allows for only the second detailed assessment of a raoellid skull. We also add extensive new data on the dental morphology of *Khirtharia inflata*, which had previously only been known by a few specimens from India documenting the upper fourth premolar and molars (P4-M3, ONGC/K/9, Ranga Rao 1972; M2-M3, VPL-K-546, Kumar and Sahni 1985) and p3-4 and the lower molars (fragmentary mandible with p3-m3, ONGC/K/8, Ranga Rao 1972; mandibular fragment with p4-m3, VPL-K-546, Kumar and Sahni 1985).

Material and methods

The fossil material described in this paper was collected from the red to grey, maroon color shale of the Upper Subathu Formation at the Aiji 2 new locality located 3 km from the East Babbian Gala locality on Moghala Kalakot Rajouri Road in Kalakot area (Waqas and Rana 2020; Rana et al. 2021), India. In Kalakot, the Paleogene rocks of the Subathu Group (composed of Kakara and Subathu formations) generally overlie the Precambrian Sirban limestone (Bhandari and Agarwal 1966). The Subathu Group represents the last phase of the existence of the Tethys Sea in the northwest sub-Himalayan region (Singh 1980; Nanda and Kumar 1999; Kumar and Loyal 2006). The Subathu Group extension has been dated from the late Paleocene to the middle Eocene based on foraminifera, dinoflagellates and pollens (Singh and Andotra 2000; Singh et al. 2016). The fossils described here have been collected by one of us (MW) in the red to grey maroon shale of the Upper Subathu Formation (Rana et al. 2021), which has been assigned to the middle Eocene based on the mammalian fauna (Sahni and Khare 1971, 1973) and corroborated by foraminifera (Mathur 1978).

The two crania, GU/RJ/297 and GU/RJ/157, were originally embedded in a hardened brown/gray clay matrix and were only very partially visible on the physical specimens. A preliminary mechanical preparation of the fossil material was performed at the Garhwal University, Palaeontology laboratory, and a final preparation and photography was performed at the Royal Belgian Institute of Natural Sciences (RBINS), Brussels. The cranium was CT scanned at the μ-CT scanner facility of the Montpellier Ressource Imagerie platform (MRI) at the University of Montpellier, using an EasyTom 150 μ-CT scanner. The voxel size of the final dataset is 69.4 μm. The rostrum GU/RJ/157 was scanned at the RBINS using an EasyTom 150 μ-CT scanner with a voxel size of 23.0 μm. Segmentation and measurements were made using Avizo ® 9.3 (Thermo Fisher Scientific-FEI). Segmentation of the cranium was done by first applying the automatic thresholding tool to make an initial rough distinction among bone, unwanted bone fragments and obscuring recrystallizations. Parts of the specimen were then digitally removed slice by slice using the pencil segmentation tool by hand. Virtual restoration of the specimen GU/RJ/157 was performed after virtual separation and reassembly of all broken parts using MorphoDig Software (Lebrun and Orliac 2017) as specified by Orliac et al. (2024). Measurements of the cranium were taken using measurement tools of Avizo ® 9.3; measurements of the dental remains were taken using digital calipers. Lengths of upper teeth are the anteroposterior dimension, and widths the buccolingual dimension on the posterior side, and across the trigonid and talonid. The dental terminology follows that of Orliac and Ducrocq (2012). Terminology of cranial features follows Wible and Spaulding (2013) and Muizon et al. (2015) and includes anglicized terms from the Nomina Anatomica Veterinaria (ICVGAN 2017). All the specimens are stored in the HNB Garhwal University Paleontology laboratory under the collection name GU/RJ. The 3D models of the specimens described in this work are available online for visualization and download on the platform MorphoMuseuM, including the virtual restoration of the specimen GU/RJ/157 (Orliac et al. 2024; model ids M3#1454, M3#1455, M3#1456).

Institutional abbreviations: GU/RJ, Garhwal University, Rajouri collection, Srinagar, Uttarakhand, India; **H-GSP**, Howard University collections stored in Geological Survey of Pakistan, Islamabad, Pakistan; **ONGC/K**, Oil and Natural Gas Commission, Kalakot collection, Dehradun, India; **RR**, Ranga Rao collection.

Description

Systematic paleontology

Artiodactyla Owen, 1848
Raoellidae Sahni et al., 1981
Khirtharia Pilgrim, 1940
Khirtharia inflata (Ranga Rao, 1972)

Holotype: ONGC/K/8, right mandible with p3-m3, alveoli of c-p2.
Paratype: ONGC/K/9, fragment of left maxilla with P4-M3.
Type horizon and locality: Basal Muree near Sind (33° 14′ 30′′ N: 74° 22′ 25′′ E).

**Distribution:** Upper Subathu Formation, middle Eocene, Kalakot, north-west Himalaya.

Referred material from this study: GU/RJ/297, complete cranium with partial left dentition including P2, P4-M3 and alveoli of I1-P1 and P3, right dentition including P2, M1-M3, and alveoli of I1-P1, P3 and P4; GU/RJ/157, anterior portion of a cranium with palate and maxilla preserving the left I2-C, P2-M1, GU/RJ/197 right m2, and right I2-P1, P3-M3; GU/RJ/146, right maxilla with P3-M3; GU/RJ/179, left fragmentary mandible with m1-m3; GU/RJ/10, right maxilla dP4-M2.

Cranium

GU/RJ/297 consists of a very well-preserved cranium, complete from the anterior edge of the maxilla to the nuchal crests of the occipital face. The general shape of the skull is elongated with a long, narrow, snout, large orbits, and a post-orbital portion of the skull that is as long as the pre-orbital one. All the bones are preserved except the premaxilla and nasals, left frontal, right auditory bulla, and zygomatic arches, which are partly broken on both sides. The specimen has undergone slight lateral compression so that its overall width is artificially narrowed (Fig. 1). The snout is also slightly bent to the right. The premaxilla and nasal are partially preserved in GU/RJ/157, although badly broken. Cranial measurements are provided in Table 1.

Nasal: On the snout, most of the nasal bone of GU/RJ/297 is broken and removed by postmortem damage, giving wide exposure to the turbinals in dorsal view (Fig. 2c). Only a small distal part of the right nasal is preserved, lying between the frontal and the lacrimal bones as seen in lateral view (Fig. 2a, c). A very small part of the nasal appears to have been present on the right side, above the canine alveolus. This morphology indicates a pronounced anterior extension of the nasal (Fig. 2a, c). The shape of the nasal is confirmed by inspection of GU/RJ/157, which preserves a wide proximal part of the right and left nasal (Figs. 3, 4). There the nasal is broken in several fragments that are displaced and partially overlap. A virtual restoration reveals the general shape and extent of the nasal (Fig. 4; see also Orliac et al. 2024): it is long and slender and extends anteriorly to the level of I3 and does not contact the lacrimal bone (Fig. 2a). The posterior edges of the piriform aperture reach the anterior margin of the canine; it is, however, not possible to reconstruct the shape of the anterior tip of the nasal bone with confidence (Fig. 3, 4c).

Premaxilla: GU/RJ/157 preserves a complete premaxilla on the left side. It is elongated and bears pointed incisors, each separated by diastemata. I1-3 are in situ, but the crown of I1 is broken. I2 appears to be the largest incisor based on the relative size of the roots. I2-3 are aligned with the canine and the incisors are arranged in a widely-opened arch. The
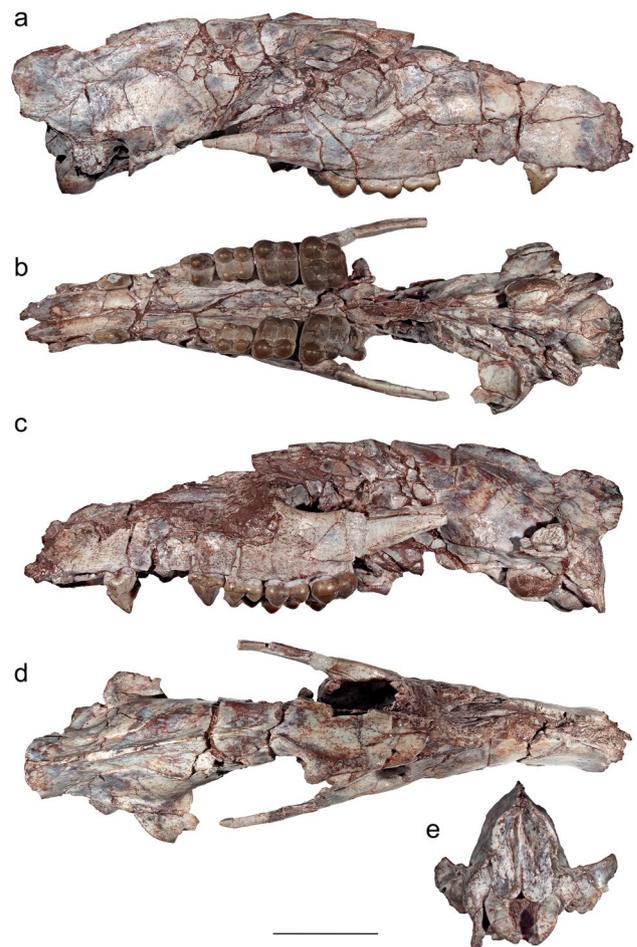
Fig. 1 Cranium of *Khirtharia inflata* (GU/RJ/297), physical specimen in right lateral (**a**), ventral (**b**), left lateral (**c**), dorsal (**d**), and posterior (**e**) views. Scale bar equals 2 cm

incisors are slightly procumbent and external. The region of the maxilla and the premaxilla at the upper canine alveolus is laterally indented (Fig. 4b). Posteriorly and dorsally, the premaxilla extends to the level of the posterior margin of P1 and meets the nasal bone (Fig. 4b). On the palate (GU/RJ/157) the suture between the premaxilla and the maxilla extends anteromedially to the lateral margin of the incisive foramen.

Maxilla: The maxilla is an elongated bone with high lateral wall. It houses the canine but the premaxilla contributes to the mesial closure of the canine alveolus. A large infraorbital foramen is located over P3. In ventral view, the palate is narrow, especially in the region of the molars, but some of this narrowness is postmortem deformation. In ventral view, the posterior margin of the maxilla is difficult to locate. A major palatine foramen opens at the level of M1, prolonged anteriorly by a major palatine sulcus; several smaller foramina open on the lateral margin of the maxilla at the M2-M3 level at the junction with the palatine (Fig. 2b).

Table 1 Cranial measurements (mm) of *Khirtharia inflata* and *Indohyus indirae* (from Patel et al 2024). * based on double measurement of left side; ** estimates based on 3D restoration (Orliac et al. 2024)

	Indohyus indirae	*Khirtharia inflata*
Maximum width across jugal arches	71.9	35.9
Maximum width across lateral bullae	35.7–34.8	17.4*
Maximum length of auditory bulla	14.8–13.5	11.4
Maximum width of auditory bulla	11.4–9.9	6.9
Width of palate between medial side of M3s	18.5–19.5	10.1**
Length from distal side of C to distal side of occipital condyle	126.6–116.9	103.5**
Maximum width across lateral side of mandibular fossae	65.8	35.6*
Maximum width across occipital condyles	20.6	13.2
Width of palate between medial sides of Cs	18.7	13**
Length from rostrum to distal side of C	38.1	17**

Fig. 2 Cranium of *Khirtharia inflata* (GU/RJ/297), labelled 3D model illustrated in right lateral (**a**), ventral (**b**), left lateral (**c**), dorsal (**d**), posterior (**e**) views. Abbreviations: **apf**, accessory palatine foramen; **dep**, oval depression; **eam**, external auditory meatus; **fm**, foramen magnum; **fpj**, frontal process of the jugal; **fr**, frontal; **gs**, glenoid surface; **iof**, infraorbital foramen; **ju**, jugal; **la**, lacrimal; **laf**, lacrimal foramen; **mp**, mastoid of the petrosal; **mpf**, major palatine foramen; **mpn**, minor palatine notch; **mps**, major palatine sulcus; **mx**, maxillary; **na**, nasal; **nuc**, nuchal crest; **oc**, occipital; **occ**, occipital condyle; **of**, optic foramen; **osof**, orbit supraorbital foramen; **pa**, parietal bone; **pap**, paroccipital process; **pgf**, postglenoid foramen; **pgp**, postglenoid process; **pop,** postorbital process; **ppt**, postpalatine torus; **ro**, root of isolated incisor; **sc**, sagittal crest; **sq**, squamosal; **sof**, supraorbital foramen; **sop**, supraoccipital process; **tb**, tympanic bulla; **tef**, temporal foramen; **tpj**, temporal process of the ugal; **tur**, turbinals. Scale bar equals 2 cm
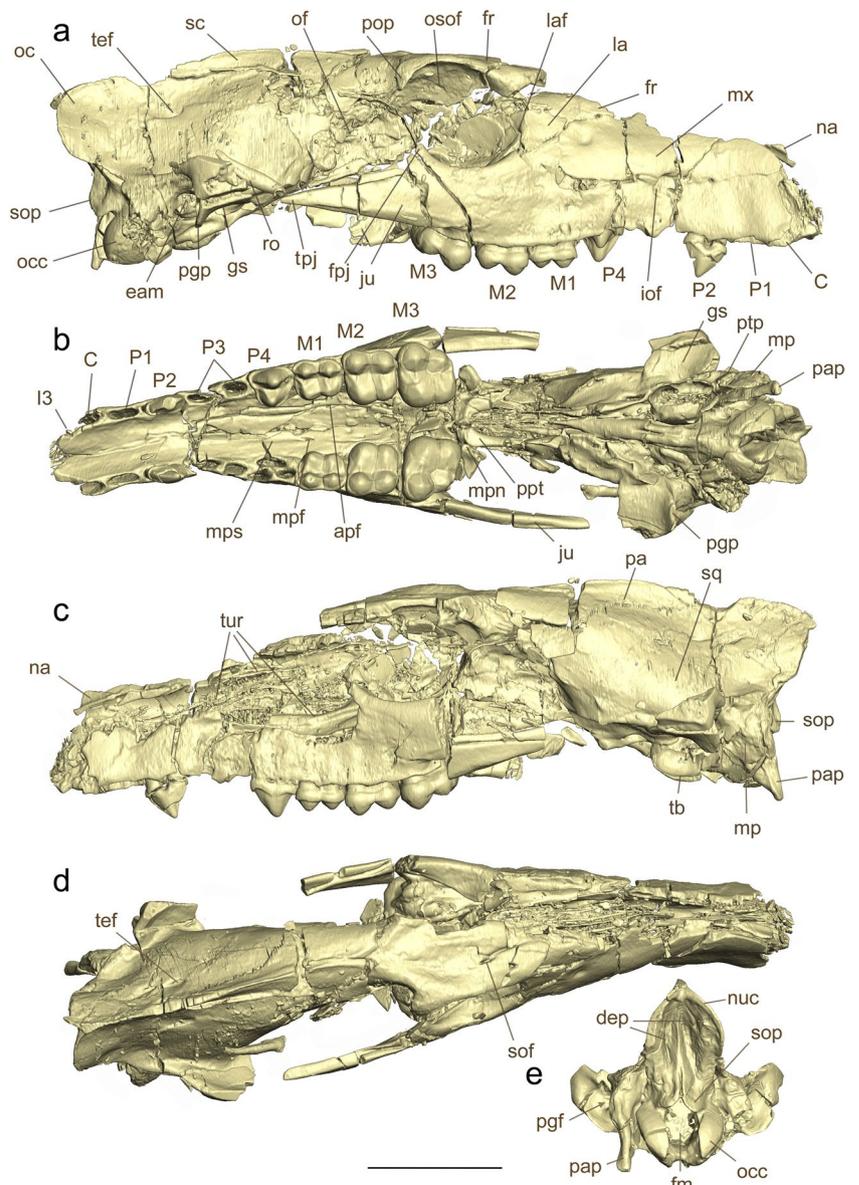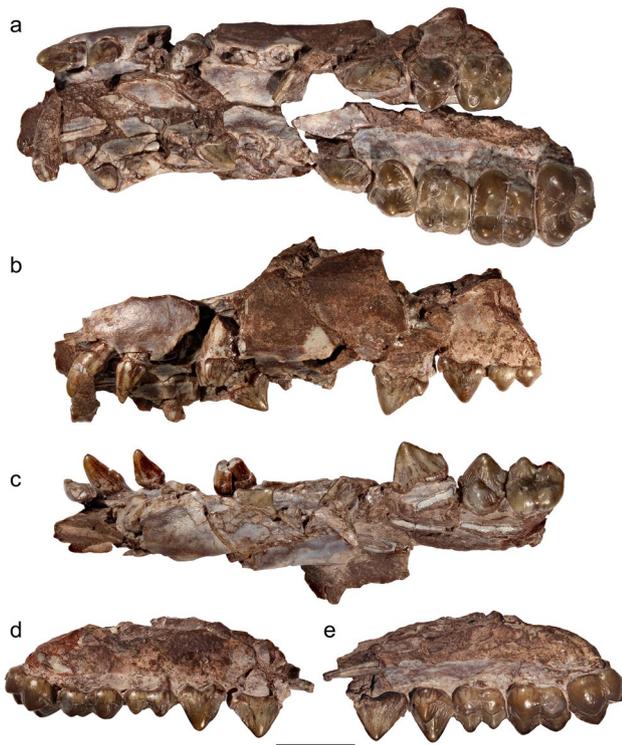
Fig. 3 Partial snout of *Khirtharia inflata* (GU/RJ/157), physical specimen illustrated in ventral (**a**), left lateral (**b**), ventral (**c**), right lateral (**d**) (right portion of the maxilla, broken off), lingual (**e**)(right portion of the maxilla, broken off) views. Scale bar equals 1 cm
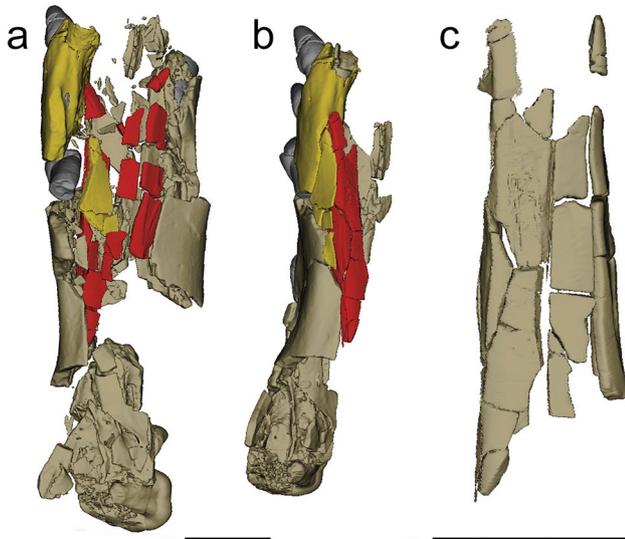
Fig. 4 Part of the specimen GU/RJ/157, anterior toward top of page. **a**. dorsal view showing the broken specimen with the premaxillary highlighted in yellow and the nasal fragments highlighted in red; **b**. dorsal view showing the restored left side of the specimen; **c**, reconstruction of the left and right nasal bones. The reconstruction process is detailed in Orliac et al. (2024). Scale bars equal 1 cm

Palatine: The limit between the palatine and the maxilla is difficult to locate precisely due to breakage in the posterior part of the palate; however, CT scan images indicate that the palatine/maxilla suture extends to the level of M1. In the posterior part of the palate, the palatine extends ventrally and bears a slender postpalatine torus (Fig. 2b), reaching the level of the occlusal surface of the molars. It is bordered laterally by a narrow minor palatine notch. The contribution of the palatine to the internal wall of the orbit is difficult to assess due to breakage.

Lacrimal: The lacrimal bone is preserved on both sides of the specimen, but best preserved on the right side. It is a sharp-edged triangular bone, contacting the maxilla and the frontal on the lateral aspect of the cranium, without overlap. It bears a lacrimal foramen on the anterior edge of the orbit on the orbital side (Fig. 2a, Online Resource 1: Fig. S1). The lacrimal foramen is prolonged anteriorly by a small nasolacrimal canal that opens into the nasal cavity; it overhangs a wide endocranial sinus that we interpreted as the maxillary sinus (Online Resource 1: Fig. S1).

Frontal: The frontal in *Khirtharia* is long anteroposteriorly and relatively slender mediolaterally and completely covers the supraorbital region and most of the orbit. The postmortem lateral compression notwithstanding, the orbits seem to have been particularly close to each other (Online Resource 1: Fig. S2: Slices 2–3). The frontal bears a deep, elongated, supraorbital foramen located in the interorbital region halfway between the median plane and the dorsal margin of the orbit. The supraorbital foramen of the orbit opens in the interorbital region, inferior and anterior to the postorbital process (Fig. 2a). It is anteriorly prolonged by a marked sulcus. The medial wall of the orbit is too damaged to identify with confidence either the limits of the bones comprising the orbital wall, or the presence of any small foramina. The shape of the supraorbital region is subrectangular in dorsal view, with a lateral protrusion of the postorbital process and a slight constriction anterior to it. The process is thick, short and blunt, and posteriorly oriented. The supraorbital region is slightly concave so that the dorsal margin of the orbit lies slightly above the mid-part; this concave area extends posterior to the postorbital process. The frontal narrows at the frontoparietal suture immediately caudal to the postorbital process. This area of the skull is extremely narrow, but the bone is particularly thick (Online Resource 1: Fig. S2 Slice 4). The frontal shows an increased thickness along its whole length (Online Resource 1: Fig. S2 Slices 3–4), especially posterior to the orbits.

Jugal: The jugal is long and slender. It forms the inferior margin of the orbit and contributes to more than half of the zygomatic arch. Anteriorly, the maxillary process (processus maxillaris) extends slightly anterior to the level of the anterior margin of the orbit. It bears a pointed frontal process (processus frontalis), the tip of which is unfortunately

broken away. Posteriorly, the temporal process (processus temporalis) of the jugal encases the zygomatic process (processus zygomaticus) of the squamosal, at the base of the frontal process. The jugal is only slightly curved, slender and shallow; its ventral margin shows only a very slight impression of the attachment site for the masseter muscle.

Parietal: The parietal forms most of the sagittal crest, the latter being slightly higher than the braincase (Fig. 2a), thin, distinct, and extending posteriorly to the supraorbital processes. Posteriorly, the parietal forms only a small part of the external wall of the braincase; it is largely hidden by the dorsal extension of the squamosal and does not contribute to the nuchal crest. A large temporal foramen opens above the level of the external acoustic meatus.

Orbitosphenoid: The orbitosphenoid can be only partly delineated. Its sutures are identified with the frontal and the alisphenoid. The optic foramen can be identified on both sides of the specimen (Figs. 2a,c) and is tall and ellipsoid in shape. It is bordered by two salient ridges and prolonged by a groove extending anteriorly toward the orbit.

Presphenoid: The presphenoid is elongate and narrow; its ventral surface is rounded and smooth. Its ventral surface has an arrow shape. Its anterior and lateral extension is difficult to assess due to breakage (Fig. 5).

Basisphenoid: The basisphenoid shares clear sutures with the presphenoid and the basioccipital. It bears the roots of the bilateral tubercles (tubercles for neck flexors, bt in Fig. 5; Nummela et al. 2006) that largely extend onto the anterior side of the basioccipital.

Alisphenoid: The alisphenoid shares sutures with the parietal, squamosal, petrosal, tympanic, presphenoid, orbitosphenoid, basisphenoid and most probably with pterygoid, although the suture with the latter is very difficult to assess. The alisphenoid extends anteriorly to the posterior margin of the sphenorbital fissure. On the ventral aspect of the cranium (Fig. 5), the alisphenoid extends from the level of the presphenoid to the anterior margin of the tympanic bulla. It encloses the foramen ovale, located at the posterior most extremity of the pterygoid process. Posterior to it, the distal margin of the alisphenoid bears the notch of the piriform fenestra; a posterior narrow process forms the anterior most part of a prominently raised joint facet for the anterior process of the tympanic. The rest of this joint facet is composed by the squamosal. The pterygoid process of the alisphenoid is badly broken and cannot be described. The ventrolateral part of the alisphenoid bears a salient crest of bone joining the anterolateral edge of the glenoid fossa to the anterior margin of the sphenoidal fissure.

Squamosal: The squamosal forms a wide part of the lateral wall of the braincase. Its suture with the parietal is visible on both side of the specimen, dorsally, it is marked by the opening of a large temporal foramen, located anterior to
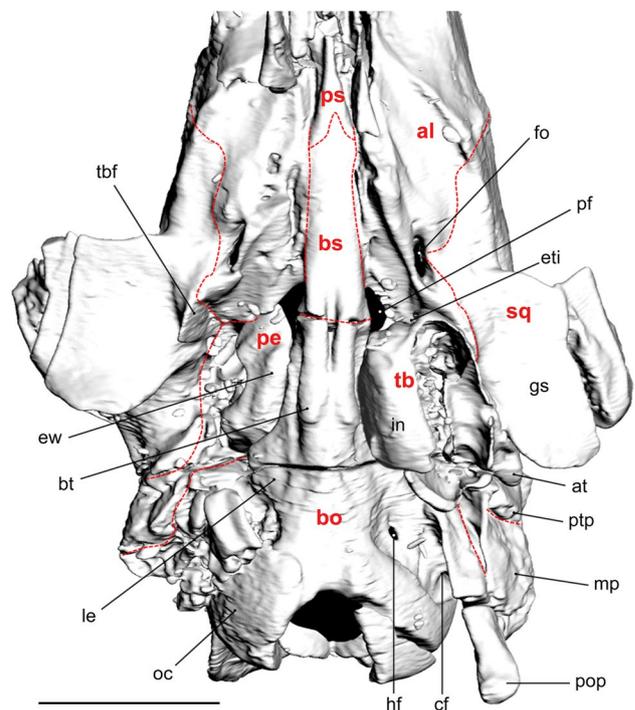
Fig. 5 Detail of the basioccipital region of GU/RJ/297, labelled 3D model in ventral view. Abbreviations: **al**, alisphenoid; **at**, auditory tube; **bo**, basioccipital; **bs**, basisphenoid; **bt**, bilateral tubercles; **cf**, condyloid foramen; **eti**, Eustaschian tube incisura; **ew**, epitympanic wing of the petrosal; **fo**, foramen ovale; **gs**, glenoid surface; **hf**, hypoglossal foramen; **in**, involucrum; **le**, lateral extension; **mp**, mastoid process of the petrosal; **oc**, occipital condyle; **pe**, petrosal bone; **pf**, pyriform fenestra; **pop**, paroccipital process; **ps**, presphenoid; **ptp**, postympanic process; **sq**, squamosal; **tb**, tympanic bulla; **tbf**, tympanic bulla facet. Bones are labeled in red and other structures in black. Scale bar equals 1 cm

the occipito-squamosal suture. Posteriorly, the squamosal forms a small portion of the nuchal crest, overhanging the paroccipital process. Laterally, the squamosal contributes to the zygomatic arch on most of its length and abut anteriorly the frontal process of the jugal. The lateroventral aspect of the squamosal bears a flat glenoid fossa, bordered posteriorly by a sharp, thin postglenoid process projecting posteroventrally. The posterior margin of the postglenoid process is pierced by a wide postglenoid foramen. The squamosal makes up the roof of the external auditory meatus, bordered posteriorly by a small postympanic process, apposed to the mastoid contribution of the paroccipital process. Ventrally, the glenoid fossa is separated from the tympanic bulla by a bony ridge of squamosal contacting the later.

Tympanic: The left tympanic is only partially preserved and most of its ventrolateral wall is broken. Its anterior part shows the incisura for the eustachian tube, while the medial part bears the bulge of the involucrum, separated from the basioccipital by the basicochlear

fissure. The lateral part of the tympanic is partly broken and reveals it is very thin. The anterolateral corner of the tympanic (anterior process of the tympanic) contacts the raised joint facet formed by the alisphenoid and the squamosal. The auditory tube is small and protrudes between the postglenoid and postympanic processes. On the posterior aspect, the posterior process of the tympanic contacts the mastoid process of the petrosal. The equivalent of the medial posterior prominence almost contacts the base of the paroccipital process of the exoccipital.

Petrosal: The ventral surface of the petrosal is partly exposed on the right side of the cranium. The promontorium is partly broken at the level of the cochlea. The posteromedial flange is wide and thick and has a small contact with the basioccipital. The mastoid portion of the petrosal is wide and wedged and intercalates between the postympanic process of the squamosal and the root of the paroccipital process of the exoccipital, laterally (Figs. 2a, 5).

Occipital: The basioccipital has a clear suture with the basisphenoid anteriorly. It is raised into a salient medial ridge. The bilateral tubercles (Nummela et al. 2006) mainly extend on the basioccipital. At the mid basioccipital, the bone is wide and seems slightly laterally projected, highlighted by the fossa underlying the occipital condyles. This lateral expansion forms the posteromedial wall of the jugular foramen. The exoccipitals bear large occipital condyles that do not touch in the median plane. The hypoglossal foramen is accompanied by one small condylar foramen laterally. The exoccipital forms an elongate paroccipital process; it is very sharp in its anterior part and contacts the auditory bulla and the part adjacent to the occipital condyle is recessed. The paroccipital process mainly projects ventrally and slightly posteriorly. On the posterior aspect of the cranium, the large foramen magnum is overhung by large bilateral processes of the supraoccipital (for the epaxial extensors of the neck, processes that project from the dorsal edge of the foramen magnum; Nummela et al.

2006). A sharp crest separating the two deep bilateral oval depressions marks the midline above the foramen magnum. The nuchal crest is salient posteriorly and projects slightly downwards.

Dentition

The complete cranium GU/RJ/297 and the maxilla GU/RJ/157 give access to most of the upper dentition of *K. inflata*. The dental formula is 3.1.4.3/3.1.4.3. The size of the teeth increases from P1-M3 on both specimens. Dental measurements are provided in Table 2. Only the base of root of I1 is preserved. The crown of I2 is relatively high and broad compared to I3. The upper incisors are unicuspid with pointed apices. Their shape is caniniform with a crown that is taller than wide. The crowns of I2 and I3 are labiolingually compressed with strongly convex labial surface. The lingual surface bears a strong cingulum and no marked endocristae (Fig. 6). The mesial and distal crests are sharp and merge with the cingulum at the mesial and distal angles of the tooth. I2 and I3 are very similar morphologically, and differ primarily in the shape of their cingulum. A long wear facet is visible on the distal crest of I3, caused by the lower canine. The three incisors are separated by small diastemata, and from the canine by a slightly larger diastema (Fig. 4c; Orliac et al. 2024: Fig. 6).

The apex of the left canine crown is broken but the angles of the mesial and distal crests indicate it was also a sharply pointed tooth. The cross section of the base of the crown is oval, and the root is massive. The base of the upper canine is wider than that of the incisors and the tooth more compressed labiolingually (Figs. 3c, 6). The lingual cingulum is continuous and flat, with fine crenulations. It prolongs on the labial surface of the crown, on the mesial and distal angles of the tooth.

The P1 is preserved only as a partial root in GU/RJ/157. It is single rooted with a longitudinal groove on the lingual surface. The P2 is double-rooted, triangular in occlusal view

Table 2 Measurements (in mm) of the upper and lower teeth of *Khirtharia inflata*. Abbreviations: **L**, length; **W**, width. * estimated value (broken tooth)

| Upper teeth	Side	I2		I3		P2		P3		P4		M1		M2		M3	
		L	W	L	W	L	W	L	W	L	W	L	W	L	W	L	W
GU/RJ/297	Left					6.92	3.16			7.15	6.59	7.70	6.71	8.81	9.14	8.89	10.51
	Right					7.01	3.20					7.81	6.12	8.65	9.05	8.68	10.49
GU/RJ/157	Left	3.70	2.10	4.20	2.90	5.98	3.10	7.35	4.87	6.83	7.31	6.89	7.49				
	Right	4.00	2.80	4.00	3.00	5.16	3.17	7.32	4.90	6.89	7.32	7.01	7.91	8.47	9.53	8.28	10.53
GU/RJ/146								7.92	3.62	6.57	7.01	6.90	7.32	8.54	8.91	8.76	10.42
GU/RJ/101												6.69	8.07	8.37	9.41	8.50	10.52
Lower teeth												m1		m2		m3	
GU/RJ/179												7.80*	5.10	8.29	6.50	10.36	7.20
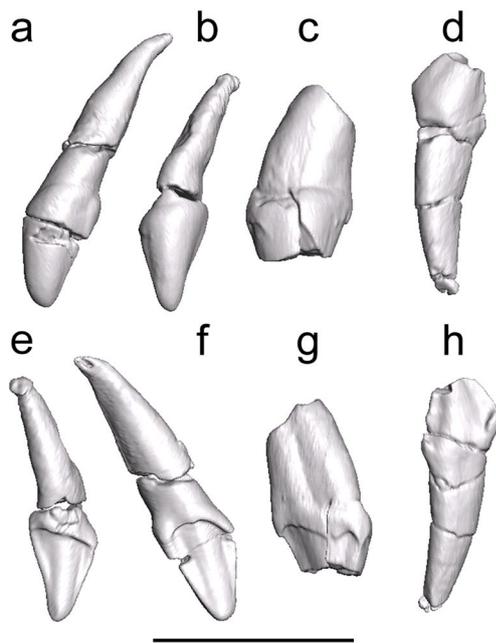
Fig. 6 Incisors and canines of GU/RJ/157 in buccal (above) and lingual (below) views. **a** and **f**, I3; **b** and **e**, I2; **c** and **g**, upper canine; **d** and **h**, putative i3. Scale bar equals 1 cm

and elongated mesiodistally (Fig. 2a, b). The crown outline is slightly concave lingually. The single main cusp, the paracone is positioned lingually and its tip is somewhat recurved distally. The paracone bears distinct pre- and postparacristae, descending from the mesiodistal sides, and merging mesially and distally to the cingulum. The cingulum completely surrounds the tooth and is raised at the distal end. The enamel of the labial surface is finely crenulated. The P3 is double-rooted and morphologically close to P2 (Fig. 3). It is higher, longer and wider than P2, especially in its distal portion. The paracone is positioned mesiocentrally and bears sharp pre- and postparacristae merging with the cingulum noted above. The enamel is ornamented with fine striations and the cingulum finely crenulated labially. A very small distostyle is present at the junction with the postparacrista. The P4 is triple-rooted, subtriangular in outline, and slightly wider than long (Fig. 3). The paracone is placed slightly distal to the protocone and a deep, narrow longitudinal valley separates both cusps. The paracone is labially convex with a lingually recurved tip inward. It bears sharp pre- and postparacristae, extended mesiodistally. The postparacrista is slightly shorter than the preparacrista, giving an asymmetrical labial profile to the crown. A small endoparacrista meets with a weak endoprotocrista located much more mesially and fused to the preprotocrista. The protocone is a large cusp; it bears a weak preprotocrista that terminates before joining the anterior cingulum. The mesiodistal surface of the tooth is rugose and strongly crenulated. The cingulum is strong and forms

a continuous shelf all along slightly elevated at the stylar regions and protocone base. The lingual lobe of the P4 of the maxilla GU/RJ/157 is more asymmetrical than that of the P4 of GU/RJ/297; it is narrower and slender in its distal part.

The molars bear low bulbous, bunodont cusps and increase in size from M1 to M3, the first molar being much smaller than M2 and M3. The M1 is narrower labiolingually than M2-3, and almost square in outline. It bears a weak paraconule merged at the basis of the preprotocrista (Figs. 1b, 2b, 3a). The cusps are moderately high, separated by transverse and longitudinal valleys. The cingulum is prominent and forms a continuous shelf around the tooth except at the lingual side. The paracone is higher than the metacone. The cristae are weak, and hypocone and styles are absent. The preparacrista is short and straight, aligned with the postparacrista and the pre- and postmetacrista (for molar cusps and crest pattern, see Online Resource 1: Fig. S3). The endoparacrista is weak but present, connected to the endoparacristule. The paraconule is small, tightly appressed to the protocone, in the continuity of the preprotocrista. It bears two faint cristae, the prepara- and endoparacristule. The preparacristule extends mesially and merges with the mesial cingulum while the endoparacristule is short and joins with the endoparacrista. The postprotocrista runs parallel to the postparacrista and contacts a very light premetacristule, delineating the outlines of the shallow and large trigon crushing basin The metaconule bears two distinct cristae, an endo- and a postmetacristule, with the former joining the endometacrista and the latter pointing towards the distal cingulum. The metacone also shows a simple pattern of cristae; the postmetacrista is short, aligned with the premetacrista and merges with the distal cingulum, the endometacrista is very light and short. The M2 is morphologically very close to the M1. The cusps are more bulbous and the premetacristule and postprotocrista are very light and worn away with little wear (Figs. 1b, 2b, 3a). The width of the tooth is wider than that of M1 and the crushing basin considerably larger. The paraconule and preprotocrista are concurrently more developed than on M1. Compared to M1-2, M3 is subtriangular, with smaller metacone and larger metaconule (Figs. 1b, 2b, 3a). The tooth bears fine crenulations all along the cingula and along the labial and labial sides of the cusps. The postmetacrista and postmetacristule join the distal cingulum and form a very little posterior lobe located labially.

The lower dentition of *Khirtharia inflata* is here documented by an incisor (Fig. 6) and a lower mandible fragment bearing m1-m3 (Fig. 7). The specimen GU/RJ/157 is associated with an ex situ incisor, stuck to the anterior most part of the premaxilla (Fig. 3a). This tooth is interpreted here as a lower incisor, as it does not match the morphology of the upper incisor (Fig. 6d, h). Besides crown morphology, the shape and curvature of the root do not correspond to that of
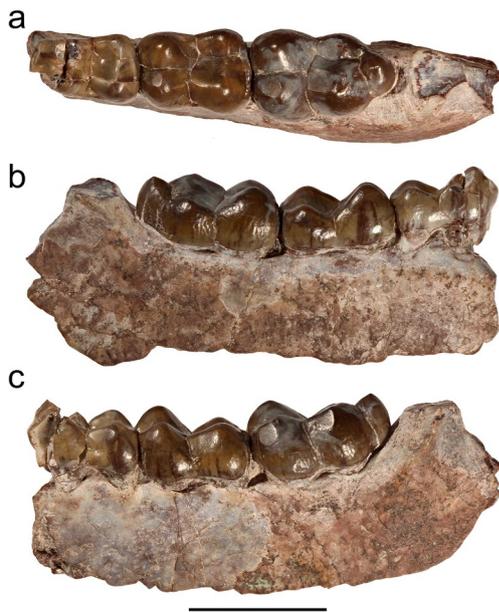
Fig. 7 Right mandible fragment of *Khirtharia inflata* bearing m1-m3 (GU/RJ/179) in occlusal (**a**), labial (**b**), and lingual (**c**) views. Scale bar equals 1 cm

the in situ root of broken I1. Compared to upper incisors, the shape of the crown is more spatulate. On the lingual side, the cingulum is not continuous and limited to the mesial and distal portion of the tooth that also bear small stylids. Given the shape of the crown and the curvature and quite large mesiodistal diameter of the root, this incisor is here tentatively refered to as a left i3.

The lower molars are documented by GU/RJ/179, a lower mandible fragment bearing m1-m3 (Fig. 7)**.** The wear of the specimen is quite advanced, but the dentine is not exposed. The cusps are bulbous and bunodont with moderately low cristids. The molars increase in size from m1 to m3 and are longer than wide. The cingulum is weak but distinct at the mesiodistal sides and slightly noticed at the protoconid/hypoconid junction, but the lingual cingulum is lacking. The paraconid is absent in all molars. The m1 is broken and maybe slightly distorted mesially. The protoconid and metaconid of the m1 are broken but nearly equal in height and closely situated. The trigonid basin is triangular, higher and markedly narrower than the talonid basin. The hypoconid is bulky and clearly larger than the other cusps, while the entoconid is greatly reduced in size. The two mesial cusps are partly broken so their cristid pattern is not clear. There are short postproto- and postmetacristid, and slightly diverging postectoproto- and postectometacristid (for molar cusps and crest pattern, see Online Resource 1: Fig. S3). The latter join the prehypo- and ectoentocristid respectively, forming the lateral and lingual edges of the crushing basin. The endohypo- and endoentocristid form the distal edge of the basin,

almost square in shape. There might be a short posthypocristid joining the distal cingulid, but its presence is difficult to ascertain because of wear. The m2 is morphologically generally similar to m1 except its size. The metaconid is slightly higher than the protoconid and both are bulbous. Crest pattern is more easily observed than in the broken m1, although it is most probably less pronounced. The protoconid bears a clear preprotocristid, joining the premetacristid at the mesial cingulid. The mesial endo- and post- cristids are very subtle and almost lost with wear. The postectocristids of the mesial lobe are discernable at the base of the cuspids. They join the prehypocristid and ectoentocristid that are higher and clearer structures, delimiting the crushing basin. The prehypocristid (cristid obliqua) connects at the protoconid base via what may be a central accessory cusp. The prehypocristid of m2 is lower and somewhat more buccal than in m1. The endocristids of the distal lobe forms a continuous transverse structure that closes the crushing basin distally. There are very subtle posthypocristid and postentocristid joining the distal cingulid. The m3 has a similar outline as m1-m2 with a general more bulbous aspect, probably due to weaker wear, and a very large hypoconulid and small entoconid. Contrary to m1-2, the trigonid of m3 is wider than the talonid. The cristids of the mesial lobe are very blunt, the postectoprotocristid is absent. The lingual edge of the crushing basin is delimited by a short and shallow postectometacristid/ectoentocristid junction. The endohypocristid/endoentocristid junction is also shallow. The posthypo- and postentocristids are faint but present. The hypoconulid is quite large and forms a distinct bulbous lobe. The cingulum is lacking all around the tooth.

Discussion

Referral of the new material and comparisons with other *Khirtharia* species

The genus *Khirtharia* was initially reported from the middle Eocene Kuldana Formation of Jahar Lammidhan, Pakistan based on a fragmentary maxilla (M1-M2) assigned to the species *Khirtharia dayi* (Pilgrim 1940). *Khirtharia*, once placed in Helohyidae (Pilgrim 1940; West 1980), Dichobunidae (Dehm and Oettingen-Spielberg 1958; Ranga Rao 1972), Choeropotamidae (Ranga Rao 1971) or even Anthracotheriidae (Sahni and Khare 1971) has subsequently been referred to Raoellidae (Theodor et al. 2007; Orliac and Ducrocq 2012) on the basis of molar morphology. The four species in *Khirtharia*: *K. dayi* (Pilgrim 1940), *K. inflata* (Ranga Rao 1972; Kumar and Sahni 1985), *K. major* (Thewissen et al. 1987) and *Khirtharia aurea* (Thewissen et al. 2001) are the most bunodont raoellids.

The species to which the material here is referred was originally described by Ranga Rao (1972) as *Bunodentus inflatus*, based on two specimens from India (ONGC/K/8 and M2 ONGC/K/9), and placed into Dichobunidae. Kumar and Sahni (1985) subsequently proposed a new combination of *Khirtharia inflatus* for the Indian material just noted and for specimens described by Sahni and Khare (1973) and referred to *Khirtharia dayi*. This attribution has then been followed by later authors (McKenna and Bell 1997; Thewissen et al. 2001; Orliac and Ducrocq 2012). According to the International Code of Zoological Nomenclature (Art. 34.2), the ending of a Latin adjectival species-group name must agree in gender with the generic name with which it is combined (Art. 31.2). If the gender ending is incorrect it must be changed accordingly (Art. 50.3.2) with the author and date of the name remaining unchanged. Therefore, the adjective *inflatus* has to be modified when transferred from a combination with the generic name *Bunodentus* of the masculine gender to a combination with *Khirtharia*, a feminine gender. The correct species name is then *Khirtharia inflata* (Ranga Rao, 1972); this corrected name has already been used by Thewissen et al. (2001) and Orliac and Ducrocq (2012).

Within *Khirtharia*, the species *Khirtharia inflata* from India and *Khirtharia dayi* from Pakistan derive from localities separated by only a few hundred kilometers. The species are very close morphologically and have been separated in the literature mostly based on the degree of bunodonty of their molars, and the height of their transverse crest. According to Thewissen et al. (1987), *Khirtharia inflata* has weaker transverse crests than *Khirtharia dayi* on upper molars, and lower molars with low bunodont cusps and crests that are

weaker than in *Khirtharia dayi*. The degree of bunodonty and crest size may be difficult to apprehend with wear and and some size variation within raoellid species should be considered (Thewissen et al. 2020). The material described here shows particularly bulbous, bunodont cusps and cuspids and is closer in size to the type and paratype of *Khirtharia inflata* (Fig. 8). We therefore refer it to the latter species. Regarding *Khirtharia aurea*, Thewissen et al. (2001) erected the species based on a single M3 from the Chorgali Formation, Pakistan. *Khirtharia aurea* distinguishes from *Khirtharia inflata* by a 30% larger size, a subtriangular outline rather than subrectangular in *Khirtharia inflata*, less bunodont cusps, better development of paraconule and cristae, conspicuous endometacristule and lack of cingulum on the lingual side. Orliac and Ducrocq (2012) referred to an isolated m3 from the middle Eocene Shanghuang Basin of China as *Khirtharia* cf. *major*. This species easily distinguishes from *Khirtharia inflata* by a much larger size.

Cranial morphology of *Khirtharia* vs. *Indohyus*

Compared to *Indohyus*, the best documented raoellid taxon, *Khirtharia* shows a more bunodont dentition with lower crowns and fewer, blunter, crests on molars. The general molar morphology of *Khirtharia* indicates less shearing than that of *Indohyus*, suggestive of different food processing (Thewissen et al. 2011). Yet, despite clear dental differences, the cranial morphology of *Khirtharia inflata* is very close to that of *Indohyus indirae* and no marked difference, apart from size (Table 1), and differences due to deformations, can be identified here. All the characteristics described
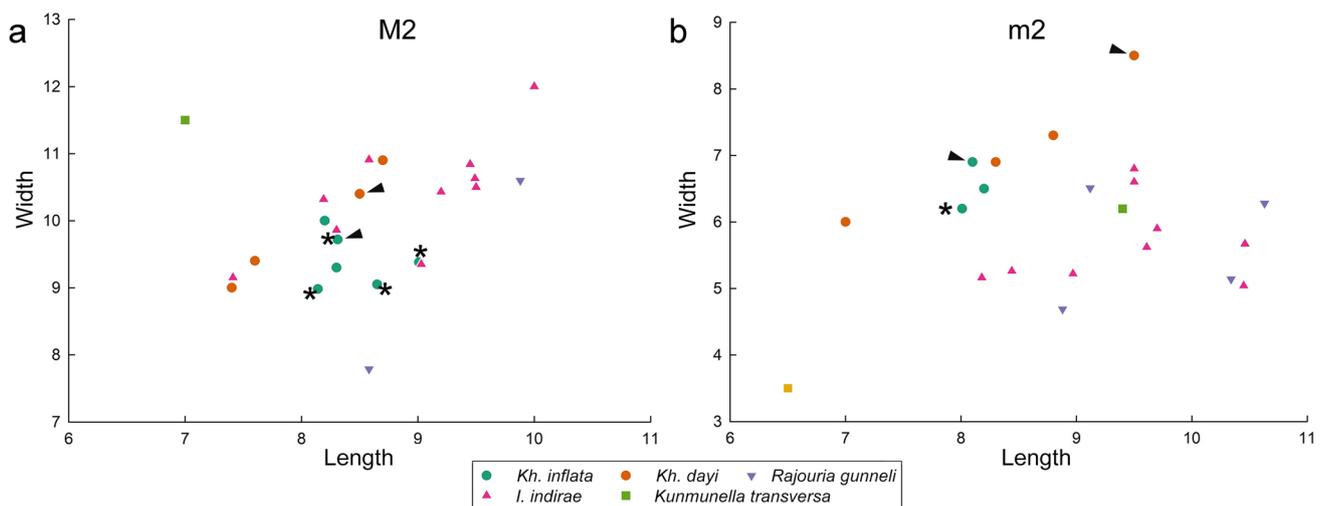
Fig. 8 Bivariate plots of length and width of upper (**a**) and lower (**b**) second molars of selected raoellid species. Type and paratype of *Khirtharia dayi* and *Khirtharia inflata* are indicated by arrows; stars indicate the bunodont specimens from Kalakot. Measurements are from the literature (Ranga Rao 1971; Sahni and Khare 1971; West 1980; Kumar and Sahni 1985; Thewissen et al. 2001; Rana et al. 2021) and available in Online Resource 1: Tables S1-2

in *Indohyus* by Patel et al. (2024) are retrieved in *Khirtharia* such as: elongated snout, opening of the infraorbital foramen located above the anterior margin of P3, intraorbital opening of the lacrimal foramen, thick blazon-shaped supraorbital region, strong postorbital constriction, triangular shape of the braincase, and thickening of the medial wall of the auditory bulla (involucrum). In this sample of two species, Raoellidae cranial morphology appears homogeneous.

We qualify our conclusion that the crania are similar given different kinds of postmortem damage in each of the two taxa with cranial material. The specimens of *Indohyus indirae* exhibit postmortem dorsoventral compression, obscuring the true morphology of the dorsoventral profile of the cranium (Online Resource 1: Fig. S4; RR 207 and RR 601 are dorsoventrally crushed, and RR 208 is obliquely medio-laterally crushed, but also with dorsoventral deformation). Due to these deformations, some of the mediolateral measurements of *Indohyus* based on RR 601 might be overestimated while obviously dorsoventral distances are inaccessible. In contrast, the *Khirtharia inflata* specimen is slightly compressed laterally, which affects mediolateral measurements and might have slightly artificially increased anteroposterior lengths. Both genera exhibit the same general cranial characteristics. The *Khirtharia* cranium is less affected by deformation and thus better completes our knowledge of Raoellidae cranial morphology. Considering the lateral compression of the specimen, the orbits of GU/RJ/297 are nevertheless closer to each other than in other terrestrial artiodactyls, recalling the pakicetid conditions (Fig. 9; see next paragraph). It is difficult to assess if the somewhat larger supraorbital width of the frontal in *Indohyus* is due to different deformations (dorso-ventral vs lateral). Yet, it is possible that the marked concavity of the frontal in *Indohyus* specimens RR 207 and RR 601 partly results from dorsoventral compression. The tube-like shape

of the postorbital portion of the cranium is also more obvious in the *Khirtharia* specimen than in the *Indohyus* specimens due to dorsoventral compression.

Some differences in cranial anatomy between the two species should be noted. *Indohyus* specimens show a higher sagittal crest than the *Khirtharia* cranium (Online Resource 1: Fig. S4). Premaxilla length is described as particularly long in *Indohyus*, with the distance between snout tip and posterior edge of the canine alveolus representing one quarter of the ventral skull length (Patel et al. 2024). Based on the specimens of *Khirtharia* described here, it seems to be smaller and would rather represent 14% of total ventral skull length (estimated total ventral length = 120 mm; tip/posterior canine length = 17 mm), which is not much different from estimates for *Diacodexis* (Russell et al., 1983: fig. 2). Unfortunately, very few complete premaxillae are preserved for early artiodactyls, limiting comparisons.

Cranial characteristics of pakicetids shared with raoellids

Nummela et al. (2006) provided a thorough description of the cranial morphology of pakicetids and highlighted the derived characteristics of this earliest family of stem cetacean. New discoveries regarding the cranial anatomy of raoellids indicates that several of these cranial characteristics are also present in this group. As mentioned by Thewissen et al. (2020) and Patel et al. (2024) and confirmed here based on observations on another raoellid genus, the incisors of raoellids are pointed, separated by diastemata and arranged on an opened arch, almost aligned with the jugal teeth row (at least for I2-3). Documentation of the premaxilla and incisors in Pakicetidae suggests the same characteristics are observed in early archaeocetes (Gingerich and Russell 1990; Nummela et al. 2006;
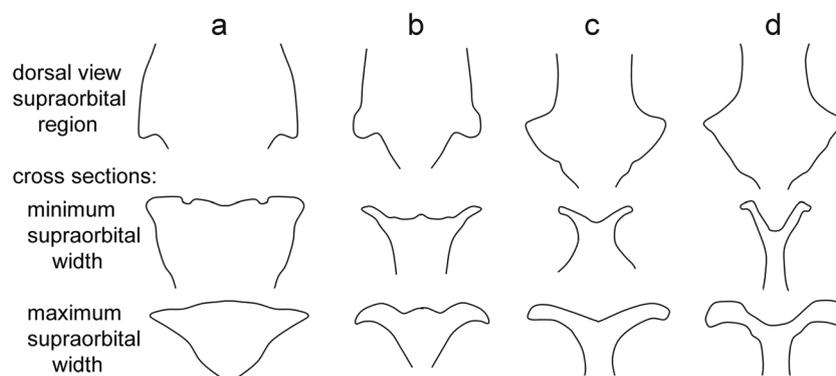
Fig. 9 Supraorbital region of Eocene dichobunid, raoellid, and archaeocete artiodactyls showing the shape of the skull at the orbit level. **a**. *Dichobune leporina* (MNHN Qu16586; Online Resource 1: Fig. S5); **b**. *Khirtharia inflata* (GU/RJ/297); **c**. *Ichthyolestes pinfoldi* (H-GSP 98134); **d**. *Pakicetus attoki* (H-GSP 96623). Drawings not to scale; they are standardized to the maximum supraorbital width. Modified from Nummela et al. (2006: fig. 3)

fig. 4A). Raoellids, however, have cingulae and cingulids on their incisors and canines, which are absent in pakicetids (Gingerich and Russell 1990).

The supra-orbital morphology of *Indohyus* and *Khirtharia* resembles that of pakicetids. The latter exhibit much variation in the supraorbital area (Nummela et al. 2006), but the orbits are convergent dorsally and the area between the orbits is recessed over the superior orbital rim (Nummela et al. 2006: figs. 3, 9). The frontal is concave and has a blazon shape in pakicetids, which is also the case in raoellids (Fig. 9). *Dichobune leporina*, hypothesized to be a fully terrestrial dichobunid (Theodor et al. 2007), shows a different shape, especially at maximum supraorbital width. This difference may be related to the shape and size of the olfactory bulbs, which are more massive and anteriorly positioned in *Dichobune* (Orliac and Thewissen 2021: fig. 4; Online Resource 1: Fig. S5). Posterior to the frontoparietal, near the sphenorbital fissure, the skulls of Pakicetidae all show a very narrow region (Nummela et al. 2006). This morphology, observed in pakicetids, ambulocetids (e.g., *Ambulocetus*; Thewissen et al. 1996), and remingtonocetids (Kumar and Sahni 1986) was proposed as an important diagnostic character of early cetaceans (Nummela et al. 2006; Thewissen et al. 2007). It is also observed, at a lesser degree, in raoellids, again most probably linked with the peculiar shape of the olfactory bulbs, elongated in raoellids (Orliac and Thewissen 2021). Yet, the elongation of the postorbital portion of the braincase is not as marked as in pakicetids, and the orbits of raoellids are not elevated as in Pakicetids.

Raoellidae and Pakicetidae also exhibit some similarities in their occipital region. Like Pakicetidae (Nummela et al. 2006) *Khirtharia* shows bilateral oval depression above the massive occipital condyle, on both sides of the salient sagittal midline (Fig. 2e). These depressions have been interpreted as insertion of the musculus longissimus capitis implied in head extension movement and could be linked to a peculiar head posture in raoellid and early cetaceans.

With respect to the auditory region and tympanic bulla morphology, in addition to the presence of a thickening of the medial wall of the tympanic bulla known as the involucrum, *Khirtharia* shares with stem cetaceans and the crown clade Cetacea the presence of a squamosal process for the bulla (Luo 1998) or raised joint facet for the anterior process of the tympanic (Nummela et al. 2006). This process, also mentioned in *Indohyus* (Patel et al. 2024), is composed of squamosal and alisphenoid in *Khirtharia* (tympanic bulla facet illustrated in Fig. 5). The presence of the sigmoid process is not easy to observe with the in situ bulla of *Khirtharia*. Rostromedially, as in pakicetids, the bulla is indented by the pathway for the Eustachian tube. Presence of the raised facet and bullar morphology should be more widely

investigated in terrestrial Eocene artiodactyl taxa to clarify the repartition of these characters within the Artiodactyla tree.

Paleoecological inferences

Paleoecology of Raoellidae has so far been investigated solely based on the species *Indohyus indirae*. It has been reconstructed as a freshwater species based on skeletal histology (Cooper et al. 2012), ear region morphology (Thewissen et al. 2007), and stable isotopes (Thewissen et al. 2007) that suggest that it spent considerable time in water. Its tooth wear resembles that of extinct stem cetaceans (Thewissen et al. 2011) and suggests similar oral processing of the food. However, isotopic studies proposed that *Indohyus* was an herbivore and not freshwater carnivore like pakicetids (Thewissen et al. 2007). Based on the new data presented here, the cranium of *Khirtharia inflata*, like *Indohyus indirae*, shows a marked increase of the bone thickness of cranium parts, especially of the frontal above and posterior to the orbit (Online Resource 1: Fig. S2; comparison with terrestrial dichobunid *Dichobune leporina* Online Resource 1: Fig. S5), but also in the occipital area (Online Resource 1: Fig. S2, Slice 8). Sutures and dentitions do not suggest that the known crania of *Khirtharia* and *Indohyus* were extremely old individuals and the thickening of the bone is not due to exostosis. On the CT scans, the bone above the orbit is compact, with some part with slight porosity, close to the medial plane, where spongy bone is present (Online Resource 1: Fig. S2k Slice 3). An incipient form of osteosclerosis was described for some postcranial elements of *Indohyus* (Cooper et al. 2012); it is also present for some parts of the cranium (Online Resource 1: Figs. S2, S5; Orliac and Thewissen 2021: fig. S2). Amson et al. (2018) described increased skull roof compactness and cranial vault thickness in the aquatic sloth *Thalassocnus* and showed that bone mass increase and pachyostosis of the cranium most probably concurred with postcranial pachyosteosclerosis in adaptation to aquatic lifestyle among tetrapods. Thick cranial vault in raoellids could therefore be another indicator of semiaquatic habits, supporting the signal carried by postcranial bones (Cooper et al. 2012).

Dorsal migration of the sense organ of the head is described in semi-aquatic animals (Barklow 2004) and in pakicetids (Nummela et al. 2006; Uhen 2007; Thewissen 2014) especially regarding orbit and nares opening position. Raoellids do not show dorsal location of the orbits, but a cross section of the orbital region shows that the orbits excavate the cranial roof and are closer to each other than in contemporaneous terrestrial artiodactyls. Regarding the external nares opening location, *Khirtharia* do not show any sign of posterior location of nostrils based on the morphology of the nasal (Fig. 5; Orliac et al. 2024: fig. 4). The location of

the external auditory meatus and the shape of the squamosal bone around it do not indicate any dorsal displacement of ear either. Thus, *Khirtharia* does not show particular signs of amphibious disposition of the sense organs; however, the disposition of the orbit, together with the long snout could reflect activity in water. The morphology of the occipital face shows a deep insertion for the *musculus longissimus capitis* (Nummela et al. 2006) implied in head extension movement; this could reflect a peculiar head posture in raoellid and early cetaceans, linked with aquatic habits.

Conclusion

The new material of *Khirtharia* from the Kalakot area improves our knowledge of raoellid cranial morphology and shows that, for the two known raoellid species, skull morphology is homogeneous. The *Khirtharia* specimen notably shares with *Indohyus* a long snout with raptorial incisors, a thick blazon-shaped supraorbital region, a strong postorbital constriction, a triangular shape of the braincase, a thickening of the medial wall of the auditory bulla (involucrum). These characters, also observed in extinct Paleogene stem cetaceans, may represent a synapomorphy of linking Raoellidae to total clade Cetacea, but this requires phylogenetic testing outside of the scope of our work. *Khirtharia* and *Indohyus* differ by the degree of bunodonty of their dentition and differences might be present regarding the height of their sagittal crest (higher in *Indohyus*) and the length of their premaxilla (longer in *Indohyus*). We cannot at present eliminate the possibility that differential deformations of the specimens might account for these variations. Regarding the paleoecology of Raoellidae, the thickening of some parts of the cranium, especially the frontal bone, accompanies the osteosclerosis described for the postcranial elements, and provides further supports to aquatic habits of members of this family. The raptorial morphology of the incisors and canine questions further the diet of these peculiar animals.

References

Amson E, Billet G, Muizon C de (2018) Evolutionary adaptation to aquatic lifestyle in extinct sloths can lead to systemic alteration of bone structure. Proc R Soc B 285:20180270

Barklow WE (2004) Amphibious communication with sounds in hippos, *Hippopotamus amphibius*. Anim Behav 68:1125–1132

Bhandari LL, Agarwal GC (1966) Eocene (Subathu series) of the Himalayan foothills, north India. Publ Cent Adv Stu Geol Punjab Univ 3:57–78

Cooper LN, Thewissen JGM, Bajpai S, Tiwari BN (2012) Postcranial morphology and locomotion of the Eocene raoellid *Indohyus* (Artiodactyla: Mammalia). Hist Biol 24(3):279–310

Dehm R, Oettingen-Spielberg T (1958) Paläontologische und geologische Untersuchungen im Tertiär von Pakistan. 2. Die mitteleocänen Säugetiere von Ganda Kas bei Basal in Nordwest-Pakistan. Bay Akad Wiss Math -Naturwiss Kl Abh 91:1–54

Gatesy J, Geisler JH, Chang J, Buell C, Berta A, Meredith RW, Springer MS, McGowen MR (2013) A phylogenetic blueprint for a modern whale. Mol Phylogenet Evol 66(2):479–506

Geisler JH, Uhen MD (2003) Morphological support for a close relationship between hippos and whales. J Vertebr Paleontol 23:991–996

Geisler JH, Uhen MD (2005) Phylogenetic relationships of extinct cetartiodactyls: Results of simultaneous analyses of molecular, morphological and stratigraphic data. J Mammal Evol 12:145–160

Gingerich PD, Russell DE (1990) Dentition of early Eocene *Pakicetus* (Mammalia, Cetacea). Contrib Mus Paleontol Univ Mich 28:1–20

ICVGAN (International Committee on Veterinary Gross Anatomical Nomenclature) (2017). Nomina Anatomica Veterinaria. Editorial Committee of the World Association of Veterinary Anatomists, Hanover, Ghent, Columbia (MO), Rio de Janeiro.

Kumar K, Loyal RS (2006) Excursion Guide on Sub-Himalayan Palaeogene Succession of Shimla Hills (Subathu–Dagshai–Kasauli Formations in Stratotype Area, Solan District, Himachal Pradesh). Wadia Institute of Himalayan Geology, Dehradun

Kumar K, Sahni A (1985) Eocene mammals from the Upper Subathu Group, Kashmir Himalaya, India. J Vertebr Paleontol 5:153–168

Kumar K, Sahni A (1986) *Remingtonocetus harudiensis*, new combination, a middle Eocene archaeocete (Mammalia, Cetacea) from Western Kutch, India. J Vertebr Paleontol 6:326–349

Lebrun R, Orliac MJ (2017) MorphoMuseuM: an online platform for publication and storage of virtual specimens. Paleontol Soc Pap 22:183–195

Luo Z (1998) Homology and transformation of the cetacean ectotympanic bullae. In: Thewissen JGM (ed) Evolutionary Emergence of Whales. Plenum Press, New York, pp 269–301

Mathur NS (1978) Biostratigraphical aspects of the Subathu Formation, Kumaun Himalaya. Rec Res Geol 5:96–112

McGowen MR, Gatesy J, Wildman DE (2014) Molecular evolution tracks macroevolutionary transitions in Cetacea. Trends Ecol Evol 29:336–346

McKenna MC, Bell SK (1997) Classification of Mammals Above the Species Level. Columbia University Press, New York

Muizon C de, Billet G, Argot C, Ladevèze S, Goussard F (2015) *Alcidedorbignya inopinata*, a basal pantodont (Placentalia, Mammalia) from the early Palaeocene of Bolivia: anatomy, phylogeny and palaeobiology. Geodiversitas 37(4):397–634

Nanda AC, Kumar K (1999) Excursion guide on the Himalayan Foreland Basin, Special Publication No. 2. Wadia Institute of Himalayan Geology, Dehradun

Nummela AS, Hussain ST, Thewissen JGM (2006) Cranial anatomy of Pakicetidae (Cetacea, Mammalia). J Vertebr Paleontol 26:746–759

Orliac MJ, Ducrocq S (2012) Eocene raoellids (Mammalia, Cetartiodactyla) outside the Indian Subcontinent: palaeogeographical implications. Geol Mag 149(1):80–92

Orliac MJ, Thewissen JGM (2021) The endocranial cast of *Indohyus* (Artiodactyla, Raoellidae): the origin of the cetacean brain. J Mammal Evol 28(3):831–843

Orliac MJ, Waqas M, Rana R, Smith T (2024) Virtual restoration of the snout of *Khirtharia inflata* (Raoellidae, Artiodactyla) from the middle Eocene of northwest Himalaya. MorphoMuseuM e224:1–8

Patel S, Nanda AC, Orliac M, Thewissen JG (2024). Cranial anatomy of *Indohyus indirae* (Raoellidae), an artiodactyl from the Eocene of India, and its implications for raoellid biology. Palaeontol Electron 27(1):1–14

Pilgrim GE (1940) Middle Eocene mammals from Northwest India. Proc Zool Soc Lond B 110:127–152

Ranga Rao A (1971) New mammals from Murree (Kalakot Zone) of the Himalayan foot hills near Kalakot, Jammu and Kashmir state, India. J Geol Soc India 12:125–134

Ranga Rao A (1972) New mammalian genera and species from the Kalakot zone of Himalayan foot hills near Kalakot, Jammu and Kashmir State, India. Dir Geol Oil Natural Gas Comm Dehra Dun India Spec Pap 1:1–22

Rana RS, Waqas M, Orliac MJ, Folie A, Smith A (2021) A new basal raoellid artiodactyl (Mammalia) from the middle Eocene Subathu Group of Rajouri District, Jammu and Kashmir, northwest Himalaya, India. Geobios 66:193–206

Sahni A, Khare SK (1971) Three new Eocene mammals from Rajouri District, Jammu and Kashmir. J Palaeontol Soc India 14:41–53

Sahni A, Khare SK (1973) Additional Eocene mammals from the Subathu Formation of Jammu and Kashmir. J Palaeontol Soc India 17:31–49

Singh BP, Andotra DS (2000) Barrier lagoon and tidal cycles in Palaeocene to Middle Eocene Subathu Formation, NW Himalaya, India. Tert Res 20:65–78

Singh BP, Singh YR, Andotra DS, Patra A, Srivastava VK, Guruaribam V, Sijagurumayum U, Singh GP (2016) Tectonically driven late Paleocene (57.9-54.7 Ma) transgression and climatically forced latest middle Eocene (41.3-38.0 Ma) regression on the Indian subcontinent. J Asian Earth Sci 115:124–132

Singh P (1980) The Subathu Group of India. Geosci J. Professional Paper. 1, Navjyoti Scientific Publications, Lucknow 1–92

Theodor JM, Erfurt J, Métais G (2007) The earliest artiodactyls. In: Prothero DR, Foss SE (eds) The Evolution of Artiodactyla. John Hopkins University Press, Baltimore, pp. 32–58

Thewissen JGM (2014) The Walking Whales: from Land to Water in Eight Million Years. University of California Press, Berkeley

Thewissen JGM, Cooper LN, Clementz MT, Bajpai S, Tiwari BN (2007) Whales originated from aquatic artiodactyls in the Eocene epoch of India. Nature 450(7173):1190–1194

Thewissen JGM, Gingerich PD, Russell DE (1987) Artiodactyla and Perissodactyla (Mammalia) from the Early-Middle Eocene Kuldana Formation of Kohat (Pakistan). Contrib Mus Paleontol Univ Mich 27:247–274

Thewissen JGM, Madar SI, Hussain ST (1996) *Ambulocetus natans* an Eocene cetacean (Mammalia) from Pakistan. Cour Forsch Inst Senckenberg 191:1–86

Thewissen JGM, Nanda AC, Bajpai S (2020) *Indohyus*, endemic radiation of raoellid artiodactyls in the Eocene of India and Pakistan. In: Prasad GVR, Patnaik R (eds) Biological Consequences of Plate Tectonics. New Perspectives on Post-Gondwana Break-up—A Tribute to Ashok Sahni. Springer, Cham, pp 337–346

Thewissen JGM, Sensor JD, Clementz MT, Bajpai S (2011) Evolution of dental wear during the origin of whales. Paleobiology 37:655–669

Thewissen JGM, Williams EM, Hussain SM (2001) Eocene mammal faunas from northern Indo-Pakistan. J Vertebr Paleontol 21:347–366

Uhen MD (2007) Evolution of marine mammals: back to the sea after 300 million years. Anat Rec 290:514–522

Waqas M, Rana RS (2020) New Raoellidae (Artiodactyla) from the Subathu Group (Middle Eocene), Rajouri District, Jammu and Kashmir, India and their significance. Himal Geol 41:171–182

West RM (1980) Middle Eocene large mammal assemblage with Tethyan affinities, Ganda Kas Region, Pakistan. J Paleontol 54:508–533

Wible JR, Spaulding M (2013) On the cranial osteology of the African palm civet, *Nandinia binotata* (Gray, 1830) (Mammalia, Carnivora, Feliformia). Ann Carnegie Mus 82(1):1–114